

Gastroscopy-conjugated photoacoustic and ultrasonic dual-mode imaging for detection of submucosal gastric cancer: *in vitro* study

Huaqin Wu(吴华钦), Haiyang Song(宋海洋), Yudian Huang(黄玉钿), Zhifang Li(李志芳), Shulian Wu(吴淑莲), Xiaoman Zhang(章小曼), Hui Li(李晖)

Citation: Chin. Phys. B . 2020, 29(6): 064205 . **doi:** 10.1088/1674-1056/ab84d4
Journal homepage: http://cpb.iphy.ac.cn; http://iopscience.iop.org/cpb

What follows is a list of articles you may be interested in

Gastroscopy-conjugated photoacoustic and ultrasonic dual-mode imaging for detection of submucosal gastric cancer: *in vitro* study

Huaqin Wu(吴华钦), Haiyang Song(宋海洋), Yudian Huang(黄玉钿), Zhifang Li(李志芳), Shulian Wu(吴淑莲), Xiaoman Zhang(章小曼), Hui Li(李晖)
Chin. Phys. B . 2020, 29(6): 064205 . **doi:** 10.1088/1674-1056/ab84d4

A novel particle tracking velocimetry method for complex granular flow field

Bi-De Wang(王必得), Jian Song(宋健), Ran Li(李然), Ren Han(韩韧), Gang Zheng(郑刚), Hui Yang(杨晖)
Chin. Phys. B . 2020, 29(1): 014207 . **doi:** 10.1088/1674-1056/ab5936

Multi-objective strategy to optimize dithering technique for high-quality three-dimensional shape measurement

Ning Cai(蔡宁), Zhe-Bo Chen(陈浙泊), Xiang-Qun Cao(曹向群), Bin Lin(林斌)
Chin. Phys. B . 2019, 28(10): 104210 . **doi:** 10.1088/1674-1056/ab427b

Optimized dithering technique in frequency domain for high-quality three-dimensional depth data acquisition

Ning Cai(蔡宁), Zhe-Bo Chen(陈浙泊), Xiang-Qun Cao(曹向群), Bin Lin(林斌)
Chin. Phys. B . 2019, 28(8): 084202 . **doi:** 10.1088/1674-1056/28/8/084202

Fast Fourier single-pixel imaging based on Sierra-Lite dithering algorithm

Zhen-Yu Liang(梁振宇), Zheng-Dong Cheng(程正东), Yan-Yan Liu(刘严严), Kuai-Kuai Yu(于快快), Yang-Di Hu(胡洋崠)
Chin. Phys. B . 2019, 28(6): 064202 . **doi:** 10.1088/1674-1056/28/6/064202

Gastroscopy-conjugated photoacoustic and ultrasonic dual-mode imaging for detection of submucosal gastric cancer: *in vitro* study*

Huaqin Wu(吴华钦)[1], Haiyang Song(宋海洋)[1], Yudian Huang(黄玉钿)[2], Zhifang Li(李志芳)[1], Shulian Wu(吴淑莲)[1], Xiaoman Zhang(章小曼)[1], and Hui Li(李晖)[1,†]

[1] *College of Photonic and Electronic Engineering, Fujian Normal University, Fujian Provincial Engineering Research Center for OptoElectronic Sensing Technology, Fujian Provincial Key Laboratory of Photonic Technology, Key Laboratory of Optoelectronic Science and Technology for Medicine, Ministry of Education, Fuzhou* 350007, *China*

[2] *Department of Pathology, Fuzhou First Hospital Affiliated to Fujian Medical University, Fuzhou* 350009, *China*

(Received 29 January 2020; revised manuscript received 24 February 2020; accepted manuscript online 31 March 2020)

This paper presents photoacoustic and ultrasonic dual-mode imaging for real-time detection of submucosal gastric cancer with a combination of gastroscopy. The diagnostic capacity was directly addressed via several phantoms and *ex vivo* experiments. Results demonstrated that superficial and submucosal gastric cancer can be diagnosed with a perceptible depth of 6.33 mm, a lateral accuracy of 2.23 mm, and a longitudinal accuracy of 0.17 mm though capturing the morphology of angiogenesis, which is a main character of the therioma-related change. The capability of gastroscopy-conjugated photoacoustic and ultrasonic dual-mode imaging system will own great potential in improving the clinical diagnostic rate of submucosal gastric cancer.

Keywords: photoacoustic imaging, intracavity pulsed laser irradiation, extra abdominal receiving photoacoustic signal, submucosal gastric cancer

PACS: 42.30.−d, 42.62.Be, 43.35.+d, 43.80.+p **DOI:** 10.1088/1674-1056/ab84d4

1. Introduction

Gastric cancer is one of the most common malignancies in digestive system, with a mortality of approximately 8.2% and 1 million newly diagnosed cases annually in the world.[1,2] Presently, white light endoscope (WLE) plus pathology biopsy is a conventional medical examination for gastric cancer screening with direct observation, diagnosis, and treatment.[3] However, its imaging mode based on photosensor fundamentally limits its ability to provide deep physiological and functional information for gastric tumor, especially for submucosal gastric cancer.[4] Moreover, WLE-invisible region and the practical background of clinician are restricted factors in the low diagnosis rate (less than 20%) of submucosal gastric cancer.[3] Since the multitype gastroscopies[5,6] provide more accurate information of lesion, they are generally used as further gastric cancer diagnosis to WLE. Nevertheless, their imaging volume or specificity limits its application in the diagnosis of submucosal gastric tumor.[7] In fact, considerable numbers of submucosal carcinoma are misdiagnosed by gastroscopy.[8]

Photoacoustic imaging (PAI)[9] uses photoacoustic effect[10] to provide anatomical and functional information with scalable spatial resolutions and imaging depths for cancer tissue[11–17] while an excellent signal to noise ratio is achieved.[18–22] Notably, taking intrinsic hemoglobin in cancer tissue as photoacoustic contrast agent increases the sensitivity for detecting abnormal angiogenesis, which is a main character of the therioma-related change.[23–27] Furthermore, PAI might provide accuracy invasive depth and preoperative staging for cancer diagnosis by yielding vital functional information and lymphovascular information from physiologically specific endogenous contrasts.[28–33] Most notable, the optical absorption of gastric cancer around the near infrared wavelengths is raised remarkably due to the property of hemoglobin's absorption spectrum.[16–19] Accordingly, we can determine PAI with near infrared pulsed laser to generate PA signals inside the submucosal gastric cancer higher than the surrounding normal tissues.

Recently, photoacoustic microscopy combined with ultrasound system[13,30] has explored its application in clinical imaging of digestive tract tumors. However, its scanning equipment does not sufficiently support intragastric scanning imaging. In this paper, we report a clinical diagnostic application of photoacoustic and ultrasonic dual-mode imaging combined with gastroscopy for submucosal gastric cancer characterized by evaluating the invasive depth and the morphology of cancer tissue. The related results of dual-mode imaging have been reported in our previous work,[16] in which the only difference is that we apply for diagnosing the superficial gastric tumor rather than submucosal gastric cancer. According

*Project supported by the National Natural Science Foundation of China (Grant Nos. 61675043, 81571726, and 81901787) and the Natural Science Foundation of Fujian Province, China (Grant Nos. 2018J01785 and 2018J01659).

†Corresponding author. E-mail: hli@fjnu.edu.cn

© 2020 Chinese Physical Society and IOP Publishing Ltd

to the structural characteristic of gastric tissue, the WLE was employed in our system to guide optical fiber to enter the gastric cavity through the esophagus, and a pulsed laser irradiates gastric cancer tissue intracavity to produce photoacoustic signal. More importantly, an extra abdominalacoustic transducer was employed to receive the photoacoustic signals on the left abdomen. By performing several phantoms and *ex vivo* experiments, we analyzed the photoacoustic signal intensity, the structure information, and the infiltrative depth of samples to reveal the potential of submucosal gastric cancer detection.

2. Imaging system

2.1. Principle

Angiogenesis is the symbolization of invasiveness of tumors.[26,27] When nanosecond-pulsed laser illuminated the gastric tissue, absorbed optical energy in hemoglobin caused thermoelastic expansion of the gastric tumor, and induced pressure waves were generated and propagated in the medium. The relationship between photoacoustic pressure and optical energy density can be given as follows:[34]

$$\nabla P^2(\boldsymbol{r},t) - \frac{1}{c^2}\frac{\partial^2}{\partial t^2}P(\boldsymbol{r},t) = -\frac{\beta}{C_\mathrm{p}}\frac{\partial}{\partial t}H(\boldsymbol{r},t), \tag{1}$$

where $P(\boldsymbol{r},t)$, $H(\boldsymbol{r},t)$, $\boldsymbol{r}=(x,y,z)$, β, C_p, and t denote photoacoustic pressure, optical energy density, position, thermal expansion coefficient, constant pressure specific heat capacity, and time, respectively. Optical energy density is the result of interaction between luminous flux $F(\boldsymbol{r})$ and optical absorption coefficient $\mu_\mathrm{a}(\boldsymbol{r})$. Because the laser pulse is sufficiently short, the relationship between photoacoustic pressure and light energy deposition satisfies the following equation

$$P(\boldsymbol{r}) = \Gamma\mu_\mathrm{a}(\boldsymbol{r})F(\boldsymbol{r}), \tag{2}$$

where Γ represents the Gruneisen coefficient. When optical energy density and the temperature of the medium are fixed, F and Γ can be regarded as constants. Hence, the diagnosis based on photoacoustic signals is related upon only μ_a of hemoglobin in angiogenesis.

2.2. Gastroscopy-conjugated photoacoustic and ultrasonic dual-mode imaging system

The schematic diagram of the real-time photoacoustic and ultrasonic dual-mode imaging system is shown in Fig. 1. An Nd:YAG laser (Sutelite I-10, Continnum) generated a 532-nm pulsed laser with the repetition rate of 10 Hz and the pulse width of 6 ns. The pulsed laser was sent to optical parametric oscillation (OPO) to produce 808-nm wavelength with the average laser intensity of 13 mJ/cm^2, which is below the maximum permissible exposure (MPE).[35] The 808-nm laser was coupled to a customized multimode optical fiber by a focusing lens, and then the fiber was delivered to endoscopy (GIF-LV1, Olympus) to enter the gastric cavity through the esophagus. By utilizing an imaging processing apparatus (CV-V1 (A), Olympus), the pulsed laser was guided by the endoscopy to irradiate gastric tissue directly. Additionally, the generated photoacoustic signals from gastric tissue were collected by a two-dimensional (2D) ultrasound array transducer (L14-5 W/60 Linear, Ultrasonix). The bandwidth of the array transducer is 5 MHz–14 MHz, and the focus depth ranges from 2 cm to 9 cm. The sampling rate of data acquisition is 40 MHz. In order to process the data, received photoacoustic data were transferred to a DAQ (Sonix DAQ, Ultrasonix) from the clinical US system (Sonix Tablet, Ultrasonix), and pulsed Nd:YAG laser triggered DAQ to received photoacoustic signals synchronous. In addition, the array transducer was controlled by an XY scan stage which was also controlled by stepper motor (SC300-2B, Zolix, Beijing, China). Stepper motor was controlled by the clinical US system for moving the transducer to do scanning along the x axis with a step size of 0.1 mm. At the same time, we employed the clinical US system to collect the ultrasonic signal synchronously. Finally, an improved US dynamic receive delay-and-sum algorithm was used to reconstruct the photoacoustic signals.

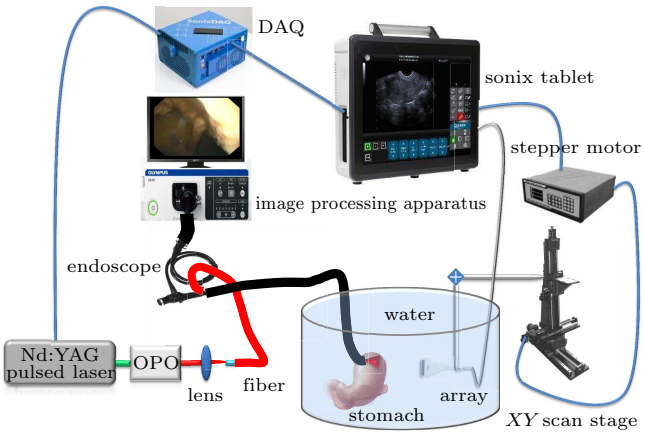


Fig. 1. The schematic diagram of real-time photoacoustic and ultrasonic dual-mode endoscopy imaging system.

3. Results

3.1. Spatial resolution

A diameter of 0.2-mm human hair was embedded in a phantom to measure the lateral and longitudinal resolutions of the system. Spatial resolutions of photoacoustic and ultrasonic dual-mode imaging system are shown in Fig. 2. The PA data and 2D PA image of the hair are shown in Figs. 2(b) and 2(c), respectively. The vertical resolution based on the full width at half maximum (FWHM) of the envelope for Hilbert-transformed vertical PA signal is estimated to be

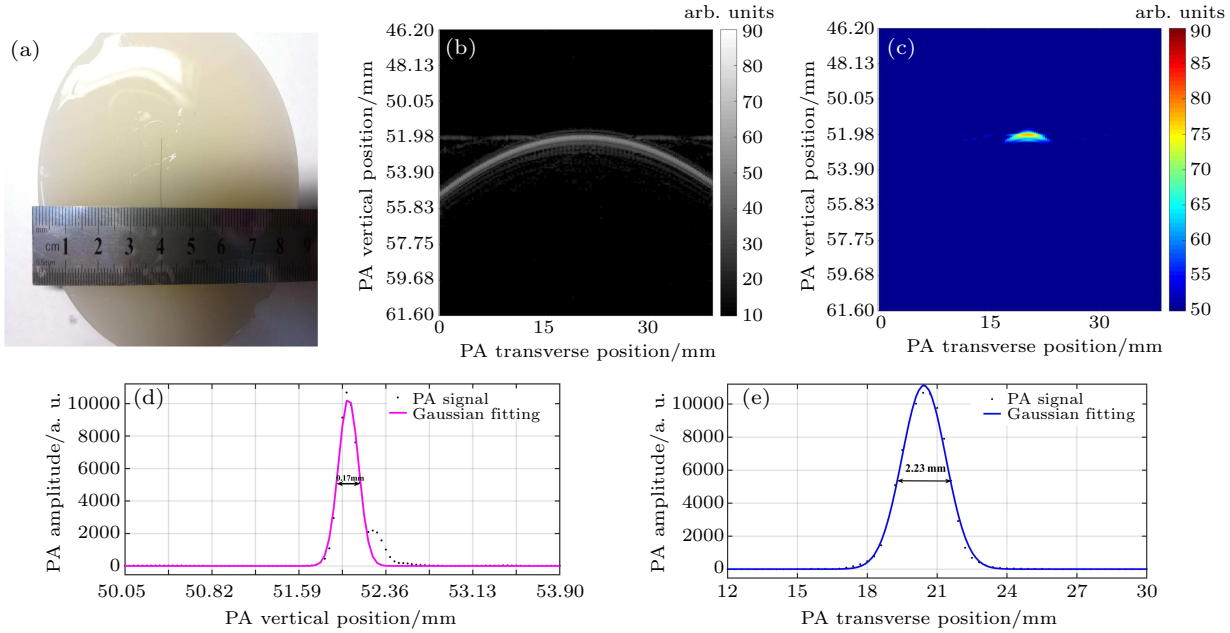


Fig. 2. Spatial resolutions of the photoacoustic and ultrasonic dual-mode imaging system. (a) Photo image of the agar with a hair; (b) PA data of the hair; (c) 2D PA image of the hair; (d) Vertical resolution of the system; (e) Transverse resolution of the system.

0.17 ± 0.08 mm, as shown in Fig. 2(d), which is accord with the theoretical value (0.26 mm, calculated by Eq. (3) in Ref. [36])

$$\boldsymbol{R}_{\mathrm{v}} = 0.88 c_{\mathrm{s}}/\Delta f, \tag{3}$$

where $\boldsymbol{R}_{\mathrm{v}}$, c_{s}, and Δf denote the vertical resolution of system, speed of sound, and the bandwidth of transducer.

In addition, the FWHM of the transverse point spread function of PA signal represents the transverse resolution of the system (2.23 ± 0.13 mm for the dual-mode imaging system), as shown in Fig. 2(e). The transverse resolution can be improved to submillimeter level by the means of deconvolution,[37,38] and so on, thereby improving the diagnostic rate of micro-gastric cancer.

3.2. Dual-mode imaging system for submucosal simulated tumors

The intensity of PA signals produced in gastric cancer is proportional to the concentration or content of hemoglobin, which is an index of angiogenic in gastric cancer. For the sake of imitating the submucosal gastric cancer, five pseudo-gastric lesions were introduced by intragastric injection of different concentrations of fresh blood and fat emulsion mixture, in consideration of the increased angiogenic nature of gastric cancer and therefore relatively increased hemoglobin levels.[39] The absorption coefficient of five simulated tumors was detected by UV VIS spectrophotometer and integrating sphere combined with KM theory[40] with five times measurements replicated, as shown in Table 1. Pseudo-gastric lesions (five simulated tumors) were introduced in a stomach, as shown in Fig. 3(a). The thinness of mucosa and muscular layers are shown in Fig. 3(d). Before the photoacoustic and ultrasonic imaging, the WLE was used to guide the tailor-made optical fiber to irradiate simulated tumors. WLE image for five simulated tumors is shown in Figs. 3(b) and 3(c).

Real-time 2D US image for simulated tumor ID 5 in Fig. 3(e) was obtained from clinical ultrasonic system. Structure information of gastric wall tissue can be accurately described. Real-time 2D PA image and dual-mode image of simulated tumor ID 5 are shown in Figs. 3(f) and 3(g), respectively. Dual-mode image can obtain the location and morphological characteristics of tumors, thus revealing the depth of invasion of tumors and the boundaries with normal tissues. Figure 3(h) shows normalized mean optical absorption and PA intensity of five submucosal simulated tumors. Aside from PA signal intensity, structure information and invasive depth of five submucosal simulated tumors were quantitatively analyzed, as shown in Fig. 3(i). Besides, signal-to-noise ratio (SNR) and contrast degree for 2D PA and US images of five submucosal simulated tumors were also quantitative analyzed, as shown in Fig. 3(j). Results show that the infiltration for tumor by PA can be discriminated at the depth of 6.33 mm with the lateral resolution of 2.23 mm and the vertical resolution of 0.17 mm. Moreover, the quantitative characterization for accurate structure features of gastric wall and the morphology of tumors, as well as the location and boundary of cancer can all be obtained. Multi-mode imaging system can obtain better SNR and contrast images than single-mode imaging in cancer detection, so that to provide more information for diagnosis.

Table 1. Parameters of five simulated tumors and the corresponding absorption coefficients.

Simulated tumor ID	Volume of blood/ml	Volume of fat emulsion/ml	Blood solubility/%	Total volume/ml	Absorption coefficient/mm^{-1}
1	0.25	0.25	50	0.5	0.133 ± 0.02
2	0.33	0.17	66.7	0.5	0.179 ± 0.04
3	0.375	0.125	75	0.5	0.199 ± 0.01
4	0.4	0.1	80	0.5	0.207 ± 0.03
5	0.5	0	100	0.5	0.260 ± 0.08

The value of absorption coefficient denotes mean ± standard deviation (SD).

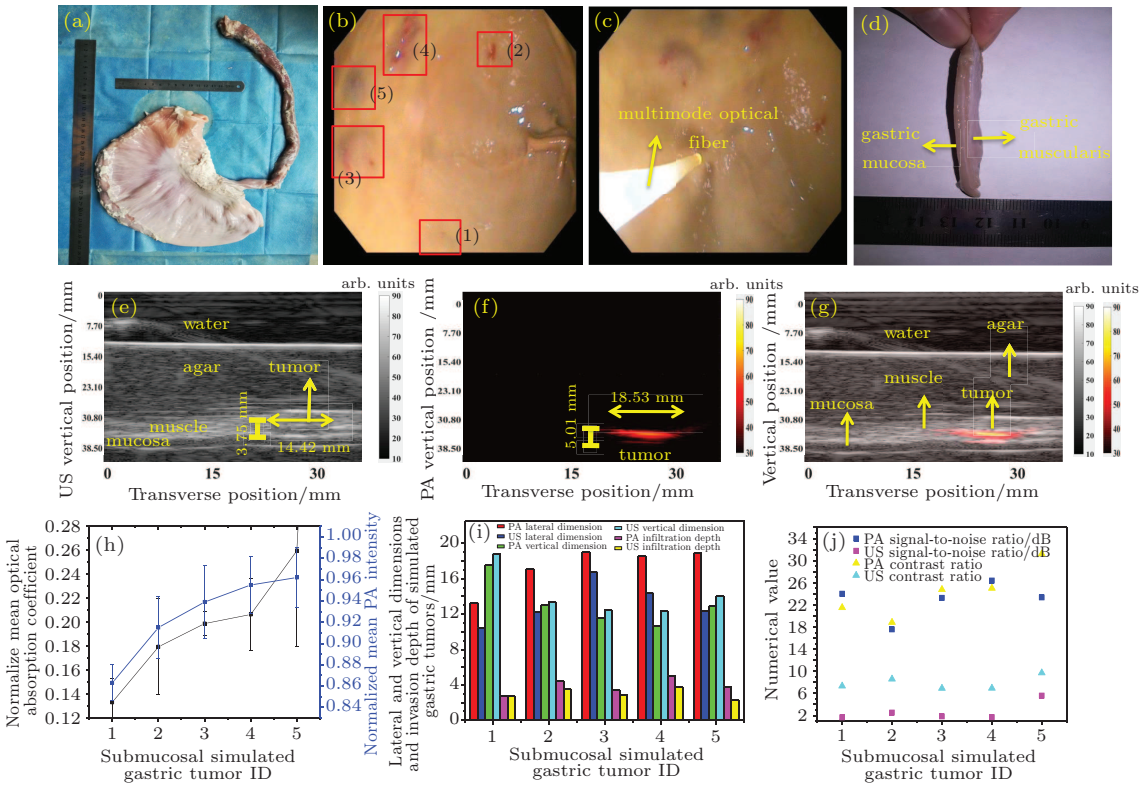


Fig. 3. Comparison between the five submucosal simulated tumors. (a) Photo image of gastric sample; (b) Photographs of five submucosal simulated tumors under endoscope; (c) Optical fiber under endoscopy; (d) Photo image of gastric wall; (e) Real-time 2D US image of simulated tumor ID 5; (f) Real-time 2D PA image of simulated tumor ID 5; (g) Real-time 2D photoacoustic and ultrasonic dual-mode imaging of simulated tumor ID 5; (h) Normalized mean optical absorption and PA intensity of five submucosal simulated tumors; (i) Structure information and infiltration depth of five submucosal simulated tumors; (j) SNR and contrast degree for 2D PA and US images of five submucosal simulated tumors.

3.3. Photoacoustic imaging of gastric cancer *in vitro*

Four gastric tumors with 2 cases poorly differentiated and 2 cases moderately differentiated *in vitro* and normal gastric tissue were added to verify the diagnostic capability and accuracy of photoacoustic imaging. All gastric samples were provided by the Pathology Department of the Fuzhou First Hospital affiliated to Fujian Medical University. All samples were obtained with patient's consent and approved by the Institutional Review Committee for clinical investigation of human subjects in biomedical research. All samples were taken from each patient and divided into two parts. One was used for histological analysis for the criteria of gastric cancer in pathology. Another one was for the *in vitro* photoacoustic study. Representative photoacoustic images for all gastric cancers and normal tissues *ex vivo* are shown in Fig. 4.

Figures 4(a) and 4(b) show the histological images of poorly differentiated adenocarcinoma and normal gastric tissue, figures 4(c) and 4(d) show the histological images of moderately differentiated adenocarcinoma and normal gastric tissue. Figures 4(e), 4(f), 4(g), and 4(h) show the photo images of corresponding samples. In addition, figures 4(i), 4(j), 4(k), and 4(l) present the reconstructed three-dimensional (3D) PA images of samples. The 3D PA images present 450 B-scan slices with 100-μm intervals for samples of each case. It is important to note that the PA intensity of gastric cancer is drastically overtopping the normal gastric tissue in reconstructed PA images on account of the tiny weak or even undetectable photoacoustic signals of normal tissues. Moreover, normalized mean PA signal intensities for all gastric cancer and normal gastric tissue were calculated, as shown in Fig. 5. Quantitative statistics show that the photoacoustic intensity of gastric cancers is also higher than that of normal tissues. The results place special emphasis on that the increased angiogenesis nature and hemoglobin level of gastric cancer tissue in support of the diagnosis of gastric cancer by photoacoustic and ultrasonic dual-mode imaging system.

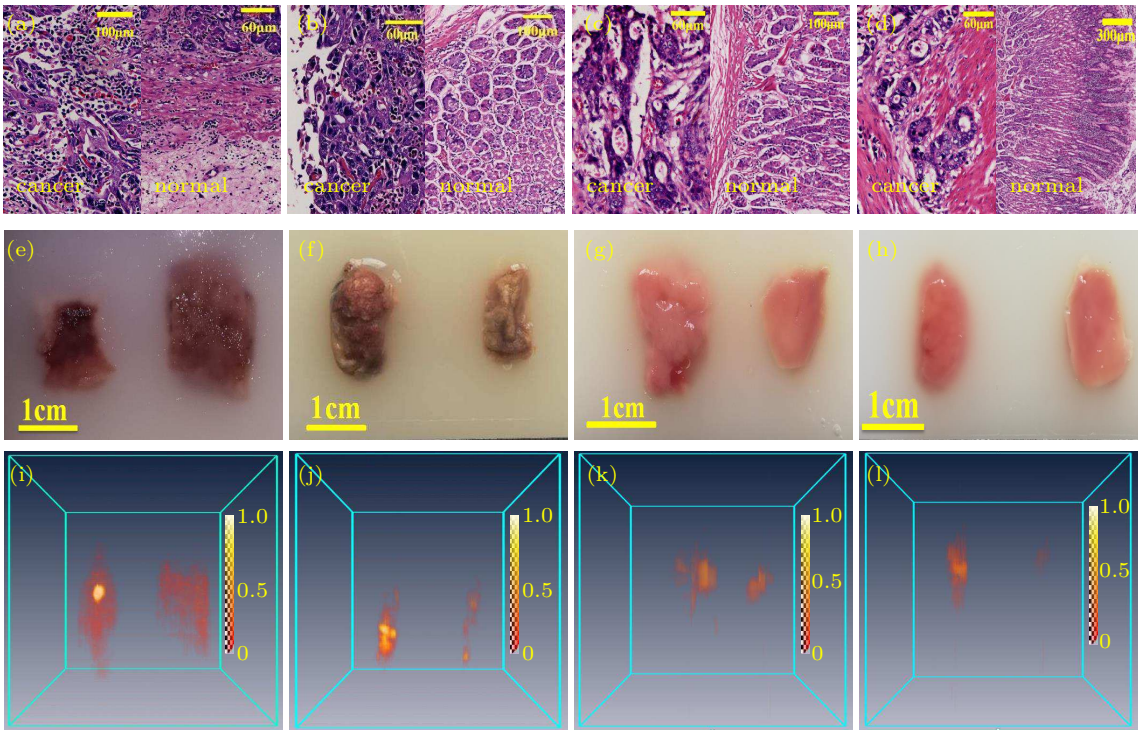


Fig. 4. Comparison between the normal gastric tissue and cancer for different degrees of differentiation. First row shows the pathological images of gastric cancer and normal tissue [panels (a), (b), (c), and (d)], second row shows the photo images [panels (e), (f), (g), and (h)]. The last row shows the corresponding reconstructed 3D PA images [panels (i), (j), (k), and (l)] of gastric cancer and normal tissue.

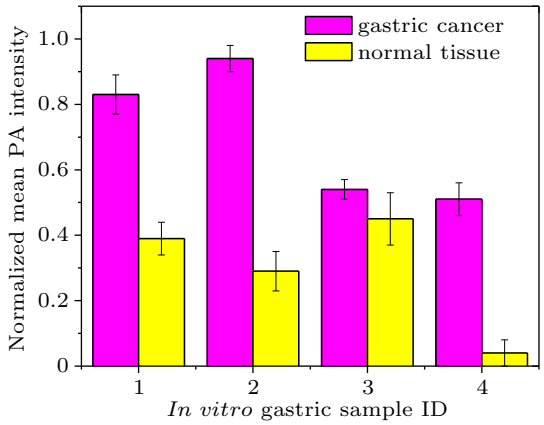


Fig. 5. Normalized mean PA intensity for all *in vitro* samples. ID 1 and ID 2 were for the poorly differentiated adenocarcinoma, ID 3 and ID 4 were for the moderately differentiated adenocarcinoma.

4. Conclusion and discussions

In this study, we proposed a gastroscopy-conjugated photoacoustic and ultrasonic dual-mode imaging method to diagnose submucosal gastric cancer by using the angiogenesis as the vinculum and the hemoglobin as the target for imaging. The level of hemoglobin, which is a significant indicator of tumor growth, aggression, and metastasis, is directly raising the optical absorption of tumor so that the specificity of photoacoustic diagnosis can be improved. The imaging results demonstrated that the infiltrative depth of submucosal gastric tumor can be realized to 6.33 mm with the lateral resolution of 2.23 mm and the vertical resolution of 0.17 mm. Moreover, the quantitative characterization for accurate structure features of gastric wall and the morphology of tumors, as well as the location and boundary of cancer can all be obtained. Benefitting from the multidimensional information provided by photoacoustic and ultrasonic dual-mode modality, the optimal treatment strategy and assessing prognosis can further be customized and selected. However, further study is still needed to improve the resolutions to identify the tumor with a size smaller than the current resolution. In addition, tissue penetration urged us to upgrade the laser system to realize centimeter-level detection of submucosal gastric cancer. Although the high metabolism of cancer can lead to higher photoacoustic signal of gastric cancer than that of normal tissue, *in vitro* gastric cancer tissue will cause blood loss during operation, thus a larger patient pool and *in vivo* study are needed to be further validated.

In summary, photoacoustic and ultrasonic dual-mode imaging with the combination of endoscopy can diagnose submucosal gastric cancer from its surrounding tissues via detecting the intensity difference of PA signals in absorption from hemoglobin. Furthermore, quantification of the precision and resolutions were demonstrated to verify the application feasibility for submucosal gastric tumor diagnosis of this approach. The capability of the dual-mode imaging system can be used for *in vivo* detection of clinical gastric cancer after further improvement. Consequently, the photoacoustic and ultrasonic dual-mode imaging with the combination of endoscopy is a promising imaging method for employing as an effective emerging diagnosis modality to increase the rate of diagnosis of superficial and submucosal gastric cancer.

References

[1] Siegel R L, Miller K D and Jemal A 2019 *CA Cancer J. Clin* **69** 7

[2] Bray F, Ferlay J, Soerjomataram I, Siegel R L, Torre L A and Jemal A 2018 *CA Cancer J. Clin* **68** 394

[3] Smyth E C, Verheij M, Allum W, Cunningham D, Cervantes A and Arnold D 2016 *Ann. Oncol Supplement* **27** v38

[4] Tashiro A, Sano M, Kinameri K, Fujita K and Takeuchi Y 2006 *World J. Gastroenterol.* **12** 4873

[5] Yu H, Yang A M, Lu X H, Zhou W X, Yao F, Fei G J, Guo T, Yao L Q, He L P and Wang B M 2015 *World J. Gastroenterol.* **21** 9156

[6] Pei Q S, Wang L, Pan J M, Ling T S, Lv Y and Zou X P 2015 *J. Gastroenterol. Hepatol.* **30** 1566

[7] Futawatari N, Kikuchi S, Sakuramoto S, Kida M and Watanabe M 2008 *Anticancer Res.* **28** 2907

[8] Alfaro E E and Gregory Y L 2011 *Adv. Anat. Pathol.* **18** 268

[9] Xu M H and Wang L V 2006 *Rev. Sci. Instrum.* **77** 041101

[10] Bell A G 1880 *Am. J. Sci.* **1880** 305

[11] Wang L V and Hu S 2012 *Science* **335** 1458

[12] Jin D, Yang F, Chen Z, Yang S and Xing D 2017 *Appl. Phys. Lett.* **111** 103703

[13] Yang J M, Favazza C, Chen R, Yao J, Cai X, Maslov K and Wang L V 2012 *Nat. Med.* **18** 1297

[14] Yuan Y, Yang S H and Xing D 2010 *Opt. Lett.* **35** 2266

[15] Wu H Q, Wang H Y, Xie W M, Wu S L, Li Z F, Zhang X M and Li H 2019 *J. Innov. Opt. Health Sci.* **12** 1950011

[16] Lin Y P, Li Z F, Li Z R, Cai J Y, Wu H Q and Li H 2018 *Opt. Commun.* **426** 519

[17] Zhang P F, Li L, Lin L, Shi J H and Wang L V 2019 *Light-Sci. Appl.* **8** 36

[18] Guo Z J, Li L and Wang L V 2009 *Med. Phys.* **36** 4084

[19] Li R, Wang P, Lan L, Frank P L, Craig J G, Chen S X and Cheng J X 2015 *Biomed. Opt. Express* **6** 1273

[20] Xu X H and Li H 2008 *Acta Phys. Sin.* **57** 4623 (in Chinese)

[21] Ishihara M Y, Masayuki S H, Akio H, Hiroshi S, Hitoshi T, Kaku I, Takatsugu W and Tomohiko A 2017 *Proc. SPIE* **10064** 100642U-1

[22] Yoon T J and Cho Y S 2013 *World J. Gastroenterol* **5** 534

[23] Choi S S, Mandelis A, Guo X X, Lashkari B, Kellnberger S and Ntziachristos V J 2016 *Biophotonics* **9** 388

[24] Valluru K S and Willmann J K 2016 *Ultrasonography* **35** 267

[25] Yamaga I, Kawaguchi S, Sakita N, Asao Y, Matsumoto Y, Yoshikawa A, Fukui T and Kanao S 2018 *Photoacoustics* **11** 6

[26] Bao S D, Wu Q L, Sathornsumetee S, Hao Y L, Li Z Z, Hjelmeland A B, Shi Q, McLendon R E, Bigner D D and Rich J N 2006 *Cancer Res.* **66** 7843

[27] Minsky B D, Mies C, Rich T A, Recht A and Chaffey J T 1988 *J. Clin. Oncol.* **6** 119

[28] Peng K, He L, Wang B and Xiao J Y 2015 *Biomed. Opt. Express* **6** 135

[29] Wang X D, William W R, Paulv L C, David P W and Fowlkes J B 2010 *Biomed. Opt. Express* **1** 1117

[30] Leng X D, J R W C, Rao B, Nandy S, Chen R M, Rais R H, Gonzalez I, Zhou Q F, Chatterjee D Y, Mutch M and Zhu Q 2018 *Biomed. Opt. Express* **9** 5159

[31] Zhang L, Zheng F, Peng Z G, Hu Z J and Yang Z 2018 *Stem. Cells Int.* **2018** 1

[32] Peng D Q, Xie W M, Wu S L, Tang J M, Li Z F and Li H 2015 *Acta Phys. Sin.* **64** 207801 (in Chinese)

[33] Yuan Y and Yang S H 2012 *Chin. Phys. B.* **21** 054211

[34] Rosencwaig A and Gersho A 1976 *J. Appl. Phys.* **47** 64

[35] Standard ANSI 2007 New York, NY: American National Standards Institute

[36] Ji X R, Xiong K D, Yang S H and Xing D 2015 *Opt. Express* **23** 9130

[37] Dixon L, Cheong F C and Grier D G 2011 *Opt. Express* **19** 16410

[38] Gurdev L L, Dreischuh T N and Stoyanov D V 1993 *J. Opt. Soc. Am. A* **10** 2296

[39] Tomaszewski M R, Gehrung M, Joseph J, Gonzalez I Q, Disselhorst J A and Bohndiek S E 2018 *Cancer Res.* **78** 5980

[40] Vargas W E and Niklasson G A 1997 *Appl. Opt.* **36** 5580